Preparation, Evaluation, and *In Vitro* Release of Folic Acid Conjugated *O*-Carboxymethyl Chitosan Nanoparticles Loaded with Methotrexate

Jingou Ji, Danjun Wu, Li Liu, Jida Chen, Yi Xu

Faculty of Pharmacy, College of Chemistry and Chemical Engineering, University of Chongqing, Chongqing 400030, China

Received 20 August 2011; accepted 25 November 2011
DOI 10.1002/app.36556
Published online in Wiley Online Library (wileyonlinelibrary.com).

ABSTRACT: To improve the targeted effect and reduce the neurotoxicity of methotrexate (MTX), folic acid (FA)-conjugated *O*-carboxymethyl chitosan (O-CMC) nanoparticles loaded with MTX were prepared via a crosslinking reaction between the carboxyl groups of *O*-CMC and Ca^{2+} ions. MTX-loaded FA–chitosan (CS) nanoparticles as controls were also prepared. The chemical structure of FA-conjugated *O*-CMC (FA–*O*-CMC) was confirmed by ^{1}H-NMR and Fourier transform infrared spectroscopy. The results show that the obtained FA–*O*-CMC nanoparticles were spherical in shape with a narrow size distribution. The encapsulation efficiency and loading capacity of MTX in the FA–*O*-CMC nanoparticles were higher than those in the FA–CS nanoparticles, and the particle size of the FA–*O*-CMC nanoparticles were also smaller than that of the control. *In vitro* release studies indicated that the release of MTX from FA–*O*-CMC nanoparticles was slower in the initial period, but the cumulative release was much higher. FA was also released from the nanoparticles; this might prove to be a potential antidote for preventing the neurotoxicity caused by MTX. © 2012 Wiley Periodicals, Inc. J Appl Polym Sci 000: 000–000, 2012

Key words: conjugated polymers; crosslinking; drug delivery systems; nanoparticle

INTRODUCTION

Methotrexate (MTX) is one of the most widely used drugs for the treatment of various neoplastic diseases, including leukemias, osteosarcoma, lymphomas, and breast cancer.[1] However, because of its nonspecific drug delivery, undesirable side effects of MTX have been reported, such as neurotoxicity and other related toxicities to normal cells.[2] Therefore, the key problem to be solved is to reduce its side effects by improving the specificity and selectivity.

Multifunctional polymeric nanoparticles, especially those that allow the targeted release of drugs in specific conditions or to sites, have immense promise in drug and gene delivery.[3–6] Folic acid (FA) is generally recognized as an effective tumor-targeting agent, as it specifically combines with folate receptors.[7] Conjugates of FA-grafting polymers or drugs could also display a high affinity property, which would enable them to rapidly bind to the folate receptors and become internalized via an endocytosis process.[8]

Polymeric materials that can conjugate with FA, such as chitosan (CS),[9,10] poly(L-lactic acid)/poly(ethylene glycol),[11] and poly(ethylene glycol)/poly(*q*-caprolactone) copolymers,[12] have been used for the formation of biodegradation nanoparticles. Among them, CS is a natural polysaccharide derived by the partial deacetylation of chitin[13,14] and has been intensively used in drug-delivery systems. However, the potential application of CS is hindered by its poor solubility in the neutral or basic pH range[15] *O*-Carboxymethyl chitosan (*O*-CMC) is a kind of water-soluble CS derivant, with the *O*-hydroxyl group of each monomer substituted by a carboxymethylic group through the ether-bond formation, and it has been proven to have favorable properties, such as low toxicity, good biocompatibility, and biodegradability.[16,17] *O*-CMC nanoparticles can be formed via the crosslinking of the carboxyl groups of *O*-CMC with calcium ions in neutral or weakly basic conditions. An increase of the pH range is expected to improve the encapsulation efficiency (EE) of acidic drugs. Furthermore, nanoparticles also display good properties for controlling drug release and delivering drugs to a target site.[18]

In addition, previous studies have supported the contention that neurotoxicity can be prevented by

Correspondence to: J. Ji (jingou_ji@yahoo.com.cn).
Contract grant sponsor: Key Scientific and Technological Projects of Chongqing Science and Technology Commission; contract grant number: CSTC2010AC5050.
Contract grant sponsor: Fundamental Research Funds for the Central Universities of China; contract grant number: CDJXS10220008.

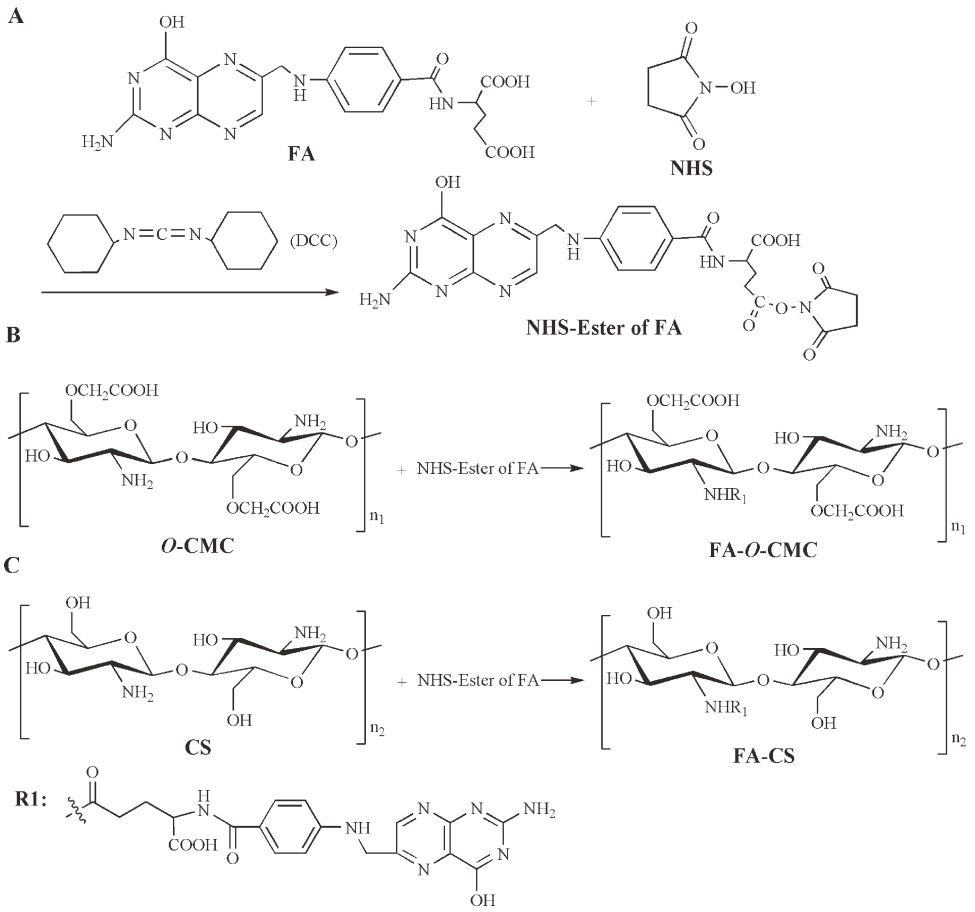

Figure 1 Scheme for the syntheses of FA–*O*-CMC and FA–CS. Synthesis processes of (A) NHS–ester of FA, (B) FA–*O*-CMC, and (C) FA–CS.

adequate FA or folinic acid rescue, even after very high doses of MTX have been administered.[19–22] Therefore, a nanoparticle system conjugated with FA may have the potential to achieve the double effects of specific targeting and assistant functions to reduce the neurotoxicity of MTX.

In this work, FA-conjugated *O*-CMC was synthesized to form nanoparticles for encapsulating the anticancer drug MTX, and MTX-loaded FA–CS nanoparticles were also prepared as controls. The physicochemical properties of the FA–*O*-CMC nanoparticles were investigated, and the *in vitro* release behaviors of MTX and FA from nanoparticles are also described.

EXPERIMENTAL

Materials

CS (deacetylation degree = 95%, molecular weight = 80 kDa) was purchased from Golden-Shell Biochemical Co., Ltd. (Zhejiang, China). *O*-CMC (90% *O*-substitution) was purchased from Qingdao Honghai Bio-Tech Co., Ltd. (Shangtung, China). Sodium tripolyphosphate (TPP) was purchased from Wenzhou Dongsheng Chemical Reagent Co., Ltd. (Zhejiang, China). MTX was supplied from Shaanxi Top Pharm Chemical Co., Ltd. (Shaanxi, China). FA, dicyclohexylcarbodiimide, and *N*-hydroxysuccinimide (NHS) were purchased from Sinopharm Chemical Reagent Co., Ltd. (Shanghai, China). All other chemicals used were analytical grade.

Synthesis of the NHS–ester of FA

The synthesis process of the NHS–ester of FA is presented in Figure 1(A). Briefly, 1.0 g of FA was dissolved in 20 mL of dimethyl sulfoxide (DMSO). A 1 : 1 molar excess of NHS and dicyclohexylcarbodiimide and 1.5 mL of triethylamine were then added. The reaction was allowed to proceed for 12 h under stirring in the dark. The byproduct dicyclohexylurea was removed by filtration. Then, the yellow NHS–ester of FA was precipitated by the dropwise addition of anhydrous ether containing 30% acetone. The product was dried *in vacuo* at room temperature.

Preparation of the FA–*O*-CMC and FA–CS conjugates

FA–*O*-CMC was prepared as follows: an *O*-CMC solution (1% w/v) was prepared by the dissolution of

O-CMC in deionized water, and an equivalent amount of the NHS–ester of FA in anhydrous DMSO was then added dropwise to the *O*-CMC solution with stirring. The reaction was held at 35°C in the dark for 12 h. FA–*O*-CMC was precipitated by the addition of excess alcohol. To isolate the conjugated polymer, the precipitate was dialyzed against phosphate buffer (pH 7.4) for 3 days and then against deionized water for 3 days. The polymer was isolated by lyophilization.

The preparation of FA–CS was performed according to the method described by Wan et al.[23] with slight changes. In brief, the NHS–ester of FA in DMSO was added to a solution of CS (0.4% w/v) in acetate buffer (pH 4.7). The resulting mixture was stirred at 35°C in the dark for 12 h. After the reaction, the pH value of the solution was adjusted to 9.0 by the dropwise addition of diluted aqueous NaOH and dialyzed first against phosphate buffer pH 7.4 for 3 days and then against deionized water for 3 days. The polymer was isolated by lyophilization.

Characterization of the FA–*O*-CMC and FA–CS conjugates

The ^{1}H-NMR spectra of the FA–*O*-CMC and FA–CS conjugates were recorded on a 500-MHz NMR spectrometer (AVANCE 500, Bruker BioSpin, Bruker Germany). With a standard procedure, the CS and FA–CS conjugate were dissolved in a CF_3COOD/D_2O mixture (0.1 mL of CF_3COOD in 0.5 mL of D_2O), and the *O*-CMC and FA–*O*-CMC conjugate were dissolved in a DCl/D_2O mixture (0.1 mL of DCl in 0.5 mL of D_2O).

The FA contents in the FA–*O*-CMC and FA–CS conjugates were determined by an ultraviolet–visible spectrophotometer (T6, Beijing Purkinje General Instrument, Beijing, China) at 358 nm (FA the molar extinction coeffcient value (ε) = 15,760 M^{-1} cm^{-1}).[24] A calibration curve of FA was made with acetic acid–sodium acetate buffer, and the degree of substitution (DS) of FA to monosaccharide residue of *O*-CMC and CS was calculated on the basis of the FA content of the final products.

Preparation of the MTX-incorporated polymeric nanoparticles

The MTX-incorporated FA–*O*-CMC nanoparticles were prepared by ionic crosslinking with $CaCl_2$. Briefly, a certain amount of MTX solution (1% w/v) in DMSO (drug-to-polymer mass ratio = 1 : 10) was added slowly to the FA–*O*-CMC solution (0.2%,w/v, pH 7.2) with sonication. The nanoparticles spontaneously formed upon addition of the $CaCl_2$ solution (0.4% w/v). Mass ratios of $CaCl_2$ to FA–*O*-CMC were selected from 1 : 7 to 1 : 4. The nanoparticle suspensions were continuously stirred for 0.5 h and centrifuged at 16,000 rpm for 30 min. The resulting nanoparticles were lyophilized and stored. Drug-free FA–*O*-CMC nanoparticles were prepared in the same way, without the addition of MTX.

The preparation of the FA–CS nanoparticles was similar to that of FA–*O*-CMC. The differences were that FA–CS was dissolved in acetic acid solution (0.2%, w/v), and the solution pH was adjusted to 5.0. Moreover, a TPP solution (0.4%, w/v) was selected as the crosslinking agent. The feeding amount of MTX and the mass ratios of TPP to FA–CS were the same as was used in the preparation of the FA–*O*-CMC nanoparticles.

Characterization of MTX-incorporated polymeric nanoparticles

The mean particle size and polydispersity index (PDI) values of the prepared FA–*O*-CMC and FA–CS nanoparticles were measured by a Nano-ZS90 zetasizer (Malvern Instruments, Malvern United Kingdom). The samples were diluted with deionized water at appropriate concentrations before they were tested.

The surface morphology of the prepared MTX-loaded FA–*O*-CMC nanoparticles was observed by transmission electron microscopy (TEM; Philips, The Netherlands) and scanning electron microscopy (SEM; Philips, The Netherlands). For TEM, the nanoparticle solution was dropped onto copper grids and dried at room temperature for imaging. For SEM, the nanoparticle suspensions were spread onto a conductive adhesive and dried at room temperature. The dried nanoparticles were then sprayed with a fine layer of gold *in vacuo*, and the images were taken.

The chemical structure and complex formation of the *O*-CMC, FA–*O*-CMC, and drug-loaded FA–*O*-CMC nanoparticles were analyzed by Fourier transform infrared (FTIR) spectroscopy (5DX/550II, Nicolet, USA). The samples were prepared as KBr pellets for IR spectroscopy investigations.

The crystal-phase constituent analysis was carried out by X-ray diffraction (XRD) and recorded by a Shimadzu Lab-XRD-6000 diffractometer (Shimadzu, Kyoto, Japan) with Cu Kα as the target at 40 kV and 30 mA. The samples were scanned from 5 to 40°.

Evaluation of the drug-loading capacity (LC) of the nanoparticles

For the determination of EE, the MTX-loaded FA–*O*-CMC and FA–CS nanoparticles were separated from the aqueous suspension media by centrifugation at 16,000 rpm for 30 min. The free amount of MTX in the supernatants was determined by UV spectrophotometry at 303 nm with the supernatant of their corresponding blank nanoparticles as the basic correction. Each batch sample was measured in triplicate.

The pellets after centrifugation were lyophilized and weighed to calculate LC. EE and LC were calculated by the following equations, respectively:

$$\mathrm{EE} = \frac{\text{Total amount of MTS} - \text{Free amount of MTX}}{\text{Total amount of MTX}} \times 100\% \quad (1)$$

$$\mathrm{LC} = \frac{\text{Total amount of MTX} - \text{Free amount of MTX}}{\text{Weight of the nanoparticles}} \times 100\% \quad (2)$$

In vitro release studies

The release of the drug-loaded nanoparticles and blank nanoparticles were studied *in vitro* by the dialysis method in phosphate-buffered saline (PBS; pH 6.8). Briefly, the lyophilized nanoparticles (30 mg) were dispersed in 3 mL of PBS (pH 6.8), and the dispersed nanoparticles were placed into a dialysis tube (molecular weight cut off = 8–14 kDa; Spectrum Bioscience, Shanghai, China) that was immersed in 30 mL of PBS solution. The system was shaken at 100 rpm and 37°C. At predefined time intervals, the release medium was collected, and equivalent fresh medium was added. The release amount of MTX from the drug-loaded nanoparticles and FA from the blank nanoparticles were determined by a UV spectrophotometer at 303 and 358 nm, respectively. Each batch sample was measured in triplicate.

RESULTS AND DISCUSSION

Synthesis and characterization of the FA–CS and FA–*O*-CMC conjugates

FA has two —COOH groups at the end positions, and it has already been established that γ—COOH of FA is more prone to this reaction because of its higher reactivity.[25] The conjugation of FA was confirmed by ^{1}H-NMR spectroscopy, as shown in Figure 2.

From the ^{1}H-NMR spectroscopy of FA–CS [Fig. 2(B)], the peaks at 2.07 ppm, attributed to the acetamino group (CH_3) and CH peak, appeared at 3.50 to 3.95 ppm and corresponded to carbons 3, 4, 5, and 6 of the glucosamine ring of CS. The peculiar signals at 7.60 and 6.40 ppm, attributed to the aromatic protons of FA, and the characteristic peaks at 6.72 and 2.45 ppm corresponded to the FA proton from H_{10} and H_{22}, respectively,[23] which indicated that FA actually attached to CS.

From the ^{1}H-NMR spectroscopy of *O*-CMC [Fig. 2(C)], the signals at 3.65, 3.81, 3.97, and 4.34 ppm, attributed to carbons 3, 4, 6, and 5 of the glucosamine ring of *O*-CMC, and the characteristic peak at 4.26 ppm corresponded to CH_2 of the carboxymethyl group.[26] The coupling of FA to *O*-CMC [Fig. 2(D)] was confirmed by the appearance of signals at 7.65 and 8.56 ppm, which corresponded to the aromatic protons and the proton at the 7 position of the pterin ring of FA, and the characteristic peaks at 2.45 ppm corresponded to the FA proton from H_{22}.[23] The relevant signals of FA were much weaker than the broad and strong proton signals of the CS and *O*-CMC residues. Therefore, for more accurate evaluation, the DS of FA was assessed by UV spectroscopy.

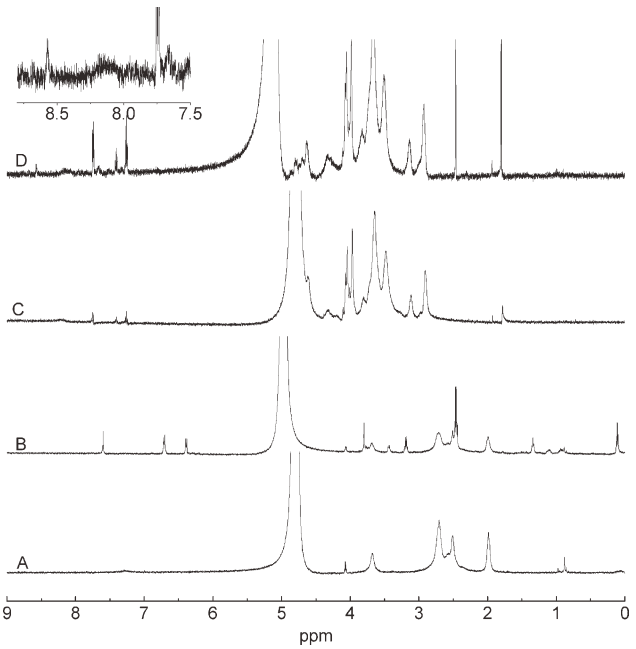

Figure 2 ^{1}H-NMR spectra of (A) CS, (B) FA–CS, (C) *O*-CMC, and (D) FA–*O*-CMC.

After the calculation based on the FA content of the final products, the DSs of FA to the monosaccharide residue of CS and *O*-CMC were 11.2 and 7.96%, respectively.

Preparation of the MTX-incorporated polymeric nanoparticles

The preparation of the drug-loaded polymeric nanoparticles with mass ratios of $CaCl_2$ to FA–*O*-CMC or TPP to FA–CS ranging from 1 : 7 to 1 : 4 was investigated. With the mass ratio of MTX to FA–*O*-CMC or FA–CS of 1 : 10, the effects of the mass ratio on the physicochemical properties of the prepared nanoparticles are shown in Tables I and II.

Table I shows that EE and LC of the FA–*O*-CMC nanoparticles increased with increasing $CaCl_2$/FA–*O*-CMC mass ratio. This trend could be explained by the fact that a larger amount of $CaCl_2$ enhanced the degree of crosslinking between the Ca^{2+} ions and free COO^- groups of FA–*O*-CMC; this led to a greater capacity to encapsulate drugs. However, a

TABLE I
Effects of the $CaCl_2$/FA–*O*-CMC Mass Ratios on the Physicochemical Properties of the FA–*O*-CMC Nanoparticles

$CaCl_2$/FA–*O*-CMC mass ratio	EE (%)	LC (%)	Particle size (nm)	PDI
1:7	28.43 ± 2.28	6.26 ± 0.61	191.2 ± 14.9	0.109 ± 0.007
1:6	31.82 ± 2.51	8.18 ± 0.82	217.4 ± 12.5	0.094 ± 0.011
1:5	41.02 ± 2.12	11.86 ± 0.94	218.7 ± 15.8	0.100 ± 0.006
1:4	50.65 ± 1.82	16.59 ± 1.37	237.2 ± 19.1	0.102 ± 0.015

The data are shown as the mean plus or minus the standard deviation. $n = 3$.

larger amount of $CaCl_2$ also increased the particle size of the nanoparticles. With the high EE and LC and the small particle size of the nanoparticles taken into consideration, the mass ratio of 1 : 5 might have been superior to the other ratios. Thus, the mass ratio of 1 : 5 was selected for the subsequent nanoparticle characterization and drug-release experiment. The values of PDI were all small; this indicated that the nanoparticles had a narrow particle size distribution and a homogeneous dispersion of FA–*O*-CMC nanoparticles.[27]

The tendency of the drug-loaded FA–CS nanoparticles was similar to that of the FA–*O*-CMC nanoparticles (Table II). However, the results revealed that EE and LC of the MTX/FA–*O*-CMC nanoparticles were higher than those of the FA–CS nanoparticles, and the particle size of the FA–*O*-CMC nanoparticles was smaller. The results might be related to the fact that the FA–CS nanoparticles were formed by crosslinking with the protonated amino group ($-NH_3^+$) of FA–CS and TPP anions, but the conjugation of FA consumed part of the amino group of CS; this reduced the crosslinking ability. However, the grafting of FA rarely affected the formation of FA–*O*-CMC nanoparticles, as the crosslinking reaction of the FA–*O*-CMC nanoparticles occurred between the Ca^{2+} ions and carboxyl groups in FA–*O*-CMC. In addition, the weakly alkaline FA–*O*-CMC solution condition might have been helpful to the improvement of EE for the weakly acidic drug MTX. The results suggest that FA–*O*-CMC was more suitable for the encapsulation of MTX than the polymeric FA–CS.

Characterization of the MTX-incorporated nanoparticles

The surface morphology of the MTX-incorporated FA–*O*-CMC nanoparticles was examined by TEM and SEM, as shown in Figure 3(A,B). The TEM image [Fig. 3(A)] showed that the nanoparticles were almost spherical in shape, with an average size of about 200 nm. The SEM image [Fig. 3(B)] coincided with the observed TEM.

The FTIR spectra of the *O*-CMC, FA–*O*-CMC, and drug-loaded FA–*O*-CMC nanoparticles are shown in Figure 4. The IR spectrum of *O*-CMC [Fig. 4(A)] showed characteristic absorption bands at 3445 cm^{-1} of multiple peaks caused by the stretching vibrations of the $-NH_2$ and —OH groups. The strong peaks at 1600 cm^{-1} and the peak at 1325 cm^{-1} were attributed to N—H bending and C—O stretching. Another strong peak at 1074 cm^{-1} corresponded to the secondary hydroxyl group C—O; this indicated that the carboxymethyl substitution occurred mainly at the C_6 position. Compared with that of *O*-CMC, the FA–*O*-CMC spectrum [Fig. 4(B)] exhibited the disappearance of the NH_2- associated band at 1600 cm^{-1} of N—H bending in the primary amine and the appearance of the NH-associated band at 1575 cm^{-1} of N—H bending in the second amine. The results indicate that the $-NH_2$ groups of *O*-CMC were partly converted into —NH groups. The strong absorption band at 1325 cm^{-1} was ascribed to the C—O bending of FA–*O*-CMC, but the absorption was weakened in the FA–*O*-CMC nanoparticles [Fig. 4(C)]; this was attributed to the linkage between the Ca^{2+} ions of

TABLE II
Effects of the TPP/FA–CS Mass Ratios on the Physicochemical Properties of the FA–CS Nanoparticles

TPP/FA–CS mass ratio	EE (%)	LC (%)	Particle size (nm)	PDI
1:7	20.07 ± 1.07	3.73 ± 0.20	270.5 ± 19.3	0.180 ± 0.008
1:6	24.56 ± 2.01	4.45 ± 0.25	291.7 ± 17.2	0.234 ± 0.062
1:5	32.77 ± 1.79	6.83 ± 0.13	340.5 ± 22.5	0.220 ± 0.045
1:4	35.02 ± 1.68	7.54 ± 0.33	357.2 ± 19.6	0.214 ± 0.039

The data are shown as the mean plus or minus the standard deviation. $n = 3$.

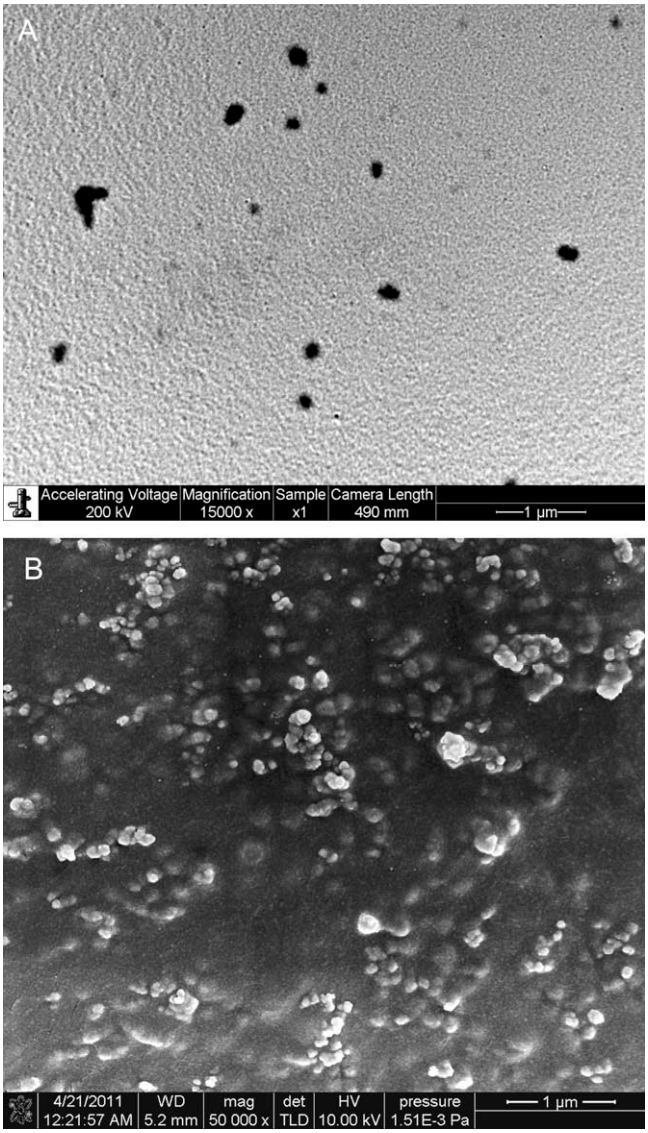

Figure 3 (A) TEM and (B) SEM images of the MTX-loaded FA–*O*-CMC nanoparticles ($CaCl_2$/FA–*O*-CMC mass ratio = 1 : 5, drug-to-polymer mass ratio = 1 : 10).

the crosslinker and the carboxyl groups of FA–*O*-CMC in the nanoparticles.[28,29] In addition, the peaks of γ(O—H) at 3445 cm^{-1} caused a slight redshift to 3425 cm^{-1} with the combination of Ca^{2+}. The characteristic absorption peaks of MTX [Fig. 4(D)] at 1604 and 1630 cm^{-1} were associated with carboxylate and amide C=O stretching.[30] The results indicate that MTX was successfully loaded into the FA–*O*-CMC nanoparticles.

Powder XRD patterns of the *O*-CMC, FA–*O*-CMC, MTX, and the MTX-loaded FA–*O*-CMC nanoparticles are illustrated in Figure 5. There was only one peak in the diffractogram of *O*-CMC at 2θ values of 20°; these indicated its crystalline nature [Fig. 5(A)]. In the prepared FA–*O*-CMC polymer [Fig. 5(B)], the intensities around 2θ = 20° decreased greatly as the crystallinity decreased, in contrast with that of

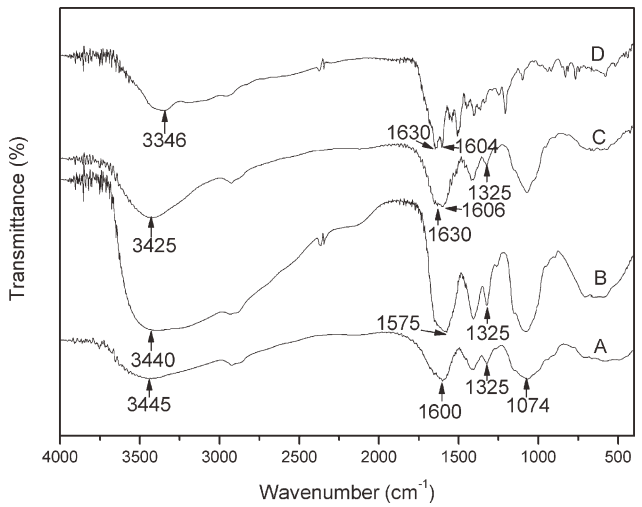

Figure 4 FTIR spectra of (A) *O*-CMC, (B) FA–*O*-CMC, (C) MTX/FA–*O*-CMC nanoparticles, and (D) MTX.

O-CMC itself, because of the deformation of the strong hydrogen bonds between *O*-CMC and FA. The novel FA–*O*-CMC polymer was amorphous in nature; this could be used to improve the biodegradability of the polymers. Nearly no peak was found in the diffractogram of the drug-loaded FA–*O*-CMC nanoparticles [Fig. 5(C)]. XRD of the FA–*O*-CMC nanoparticles showed characteristics of an amorphous polymer. The nanoparticles were composed of a dense network structure of interpenetrating polymer chains crosslinked to one another by $CaCl_2$ counterions. XRD implicated greater disarray in the chain alignment in the nanoparticles after the crosslinks.[31,32] In addition, the characteristic peaks of MTX [Fig. 5(D)] disappeared in those corresponding to the drug-loaded nanoparticles, and they overlapped with the noise of the coated polymer itself. These indicated that the drug was dispersed at the

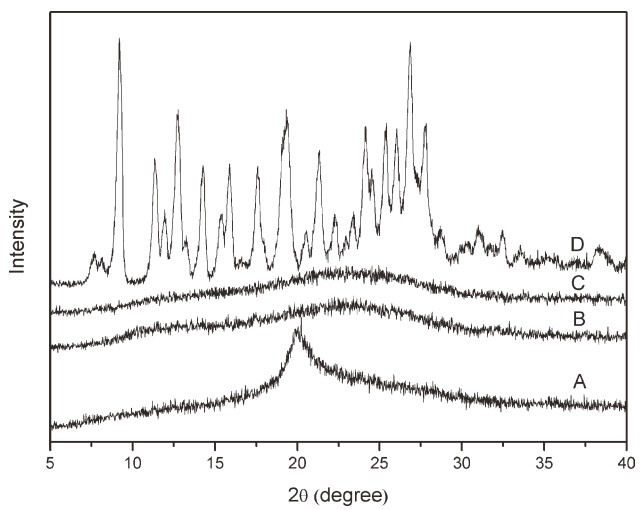

Figure 5 XRD patterns of (A) *O*-CMC, (B) FA–*O*-CMC, (C) MTX/FA–*O*-CMC nanoparticles, and (D) MTX.

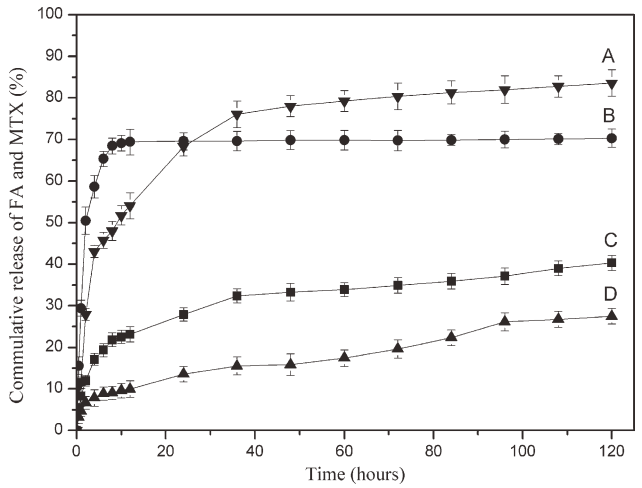

Figure 6 *In vitro* release curves of the (A) MTX from the drug-loaded FA–*O*-CMC nanoparticles and (B) FA–CS nanoparticles and the release of FA from the (C) blank FA–CS nanoparticles and (D) FA–*O*-CMC nanoparticles ($n = 3$).

molecular level in the polymer matrix, and hence, no crystals were found in the drug-loaded matrices.[33]

In vitro release studies

The study of the *in vitro* release behaviors of the drug-loaded polymeric nanoparticles (drug-to-polymer ratio = 1 : 10, and mass ratio of crosslinking agent to polymer = 1 : 5) and the corresponding blank nanoparticles was carried out at pH 6.8. As the surrounding of tumor mass has a slightly acidic pH around 6.8, it was interesting to study how the drug-release profiles progressed at this particular pH.[34]

The *in vitro* release profiles of MTX [Fig. 6(A,B)] appeared to have three phases.[35] The first phase was a rapid release or burst release in the first period. The rapid initial release involved the diffusion of the bound or adsorbed drug at the surface of the nanoparticles. The release of MTX from the FA–CS nanoparticles was relatively faster than that from the FA–*O*-CMC nanoparticles; this may have been related to the lower crosslinking ability of the FA–CS nanoparticles. About 50 and 28% of MTX were released from the FA–CS and FA–*O*-CMC nanoparticles, respectively, in this phase (within the first 2 h). The second phase was a relatively slow release, ranging from 2 to 24 h, which could have been caused by a pore diffusion mechanism of the drug out of the nanoparticles into the external environment. Moreover, the particle size of the drug-loaded FA–CS nanoparticles was larger than that of the FA–*O*-CMC nanoparticles, and the larger size also increased the rate of fluid ingress into the matrix. The third phase was a slower release that depended on the degradation of the polymer. The cumulative release of MTX from the drug-loaded FA–CS and FA–*O*-CMC nanoparticles showed 70 and 83% releases at the end of the 5th day, respectively. The results reveal that the cumulative release of MTX from the drug-loaded FA–*O*-CMC nanoparticles was higher than that from the FA–CS nanoparticles. This might have been due to the fact that FA–*O*-CMC could dissolve in the approximately neutral release medium (pH 6.8), but FA–CS was insoluble in the neutral or weakly basic pH range. The results indicate that the FA–*O*-CMC nanoparticles might have had better bioavailability.

In addition, previous study has supported the contention that neurotoxicity can be prevented by adequate FA or folinic acid rescue, even after very high doses of MTX have been administered. In this nanoparticle system, FA not only acted as the targeting reagent in the progress of drug delivery but also played the potential role of antidote to prevent the neurotoxicity of MTX. The release curves of the blank FA–CS and FA–*O*-CMC nanoparticles are shown in Figure 6(C,D). The results show that FA could release from the nanoparticles, and the release of FA from the blank FA–CS nanoparticles was faster than that from the FA–*O*-CMC nanoparticles. This may have been related to the higher substitution degree of the FA–CS conjugate. Slowly released FA might be a potential antidote to prevent the neurotoxicity caused by MTX.

CONCLUSIONS

To improve tumor-cell-selective targeting and prevent MTX-induced host toxicity, MTX-encapsulated FA–*O*-CMC nanoparticles were prepared. The obtained MTX-loaded FA–*O*-CMC nanoparticles were spherical in shape with a narrow particle size distribution. EE and LC of MTX in the FA–*O*-CMC nanoparticles were higher than those in the FA–CS nanoparticles, and the particle size of the FA–*O*-CMC nanoparticles were also smaller, as the mass ratios of crosslinking agent to polymer varied from 1 : 7 to 1 : 4. The *in vitro* release studies of the FA–CS and FA–*O*-CMC nanoparticles indicated that a slower drug release from the FA–*O*-CMC nanoparticles was observed in the initial period, but the cumulative release of MTX from the drug-loaded FA–*O*-CMC was higher than that from the FA–CS nanoparticles. FA could release from the blank nanoparticles; these could be used as an antidote to reduce the neurotoxicity caused by MTX. The experimental results suggested that the FA–*O*-CMC nanoparticles have highly promising potential as drug carriers for MTX therapy in cancers.

References

1. Yang, X. D.; Zhang, Q. Q.; Wang, Y. S.; Chen, H.; Zhang, H. Z.; Gao, F. P.; Liu, L. R. Colloids Surf B 2008, 61, 125.

2. Seo, D. H.; Jeong, Y. I.; Kim, D. G.; Jang, M. J.; Jang, M. K.; Nah, J. W. Colloids Surf B 2009, 69, 157.
3. Wang, H. J.; Zhao, P. Q.; Liang, X. F. Biomaterials 2010, 31, 4129.
4. Veiseh, O.; Gunn, J. W.; Zhang, M. Q. Adv Drug Delivery Rev 2010, 62, 284.
5. Liang, X. F.; Wang, H. J.; Jiang, X. G.; Chang, J. J Nanopart Res 2010, 12, 1723.
6. Shi, X. W.; Du, Y. M.; Yang, J. H. J Appl Polym Sci 2006, 100, 4689.
7. Sudimack, J.; Lee, R. J. Adv Drug Delivery Rev 2000, 41, 147.
8. Leamon, C. P.; Reddy, J. A. Adv Drug Delivery Rev 2004, 56, 1127.
9. Mansouri, S.; Cuie, Y.; Winnik, F.; Shi, Q.; Lavigne, P.; Benderdour, M.; Beaumont, E.; Fernandes, J. C. Biomaterials 2006, 27, 2060.
10. Wang, H. J.; Zhao, P. Q.; Liang, X. F.; Gong, X. Q.; Song, T.; Niu, R. F.; Chang, J. Biomaterials 2010, 31, 4129.
11. Lee, E. S.; Na, K.; Bae, Y. H. J Controlled Release 2003, 91, 103.
12. Park, E. K.; Kim, S. Y.; Lee, S. B.; Lee, Y. M. J Controlled Release 2005, 109, 158.
13. Ji, J. G.; Hao, S. L.; Wu, D. J.; Huang, R.; Xu, Y. Carbohydr Polym 2011, 85, 803.
14. Manchanda, R.; Nimesh, S. J Appl Polym Sci 2010, 118, 2071.
15. Sun, Y.; Wan, A. J. J Appl Polym Sci 2007, 105, 552.
16. Jayakumar, R.; Prabaharan, M.; Nair, S. V.; Tokura, S.; Tamura, H.; Selvamurugan, N. Prog Mater Sci 2010, 55, 675.
17. Liu, Z. H.; Jiao, Y. P.; Zhang, Z. Y. J Appl Polym Sci 2007, 103, 3164.
18. Anitha, A.; Maya, S.; Deepa, N.; Chennazhi, K. P.; Nair, S. V.; Tamura, H.; Jayakumar, R. Carbohydr Polym 2011, 83, 452.
19. Cohen, I. J. J Pediatr Hematol Oncol 2004, 26, 156.
20. Cohen, I. J. Med Hypotheses 2007, 68, 1147.
21. Bayram, M.; Ozogul, C.; Ercan, Z. S.; Dilekoz, E.; Soyer, C.; Bayram, O. Adv Ther 2006, 23, 772.
22. Flombaum, C. D.; Meyers, P. A. J Clin Oncol 1999, 17, 1589.
23. Wan, A. J.; Sun, Y.; Li, H. L. Int J Biol Macromol 2008, 43, 415.
24. Stella, B.; Arpicco, S.; Peracchia, M. T.; Desmaële, D.; Hoebeke, J.; Renoir, M.; D'Angelo, J.; Cattel, L.; Couvreur, P. J Pharm Sci 2000, 89, 1452.
25. Zhang, Z. P.; Lee, S. H.; Feng, S. S. Biomaterials 2007, 28, 1889.
26. Wang, Y. S.; Liu, L. R.; Weng, J.; Zhang, Q. Q. Carbohydr Polym 2007, 69, 597.
27. Ji, J. G.; Hao, S. L.; Liu, W. Q.; Wu, D. J.; Wang, T. F.; Xu, Y. Colloid Surf B 2011, 83, 103.
28. Anitha, A.; Divya Rani, V. V.; Krishna, R.; Sreeja, V.; Selvamurugan, N.; Nair, S. V.; Tamura, H.; Jayakumar, R. Carbohydr Polym 2009, 78, 672.
29. Sun, S. L.; Wang, A. Q. J Hazard Mater 2006, 131, 103.
30. Dhanikula, R. S.; Hildgen, P. Biomaterials 2007, 28, 3140.
31. Wan, A. J.; Sun, Y.; Li, H. L. J Appl Polym Sci 2009, 114, 2639.
32. Yoksan, R.; Jirawutthiwongchai, J.; Arpo, K. Colloids Sur B 2010, 76, 292.
33. Rokhade, A. P.; Agnihotri, S. A.; Patil, S. A.; Mallikarjuna, N. N.; Kulkarni, P. V.; Aminabhavi, T. M. Carbohydr Polym 2006, 65, 243.
34. Dev, A.; Mohan, J. C.; Sreeja, V.; Tamura, H.; Patzke, G. R.; Hussain, F.; Weyeneth, S.; Nair, S. V.; Jayakumar, R. Carbohydr Polym 2010, 79, 1073.
35. Agnihotri, S. A.; Aminabhavi, T. M. J Controlled Release 2004, 96, 245.